

# Resolved photometry of Young Massive Clusters in the starburst galaxy NGC 4214<sup>\*</sup>

A. Sollima<sup>1†</sup>, M. Cignoni<sup>1,2</sup>, R. G. Gratton<sup>3</sup>, M. Tosi<sup>1</sup>, A. Bragaglia<sup>1</sup>,  
S. Lucatello<sup>3</sup>, G. Meurer<sup>4</sup>

<sup>1</sup> *INAF Osservatorio Astronomico di Bologna, via Ranzani 1, Bologna, 40127, Italy*

<sup>2</sup> *Dipartimento di Astronomia, Università di Bologna, via Ranzani 1, Bologna, 40127, Italy*

<sup>3</sup> *INAF Osservatorio Astronomico di Padova, vicolo dell'Osservatorio 5, Padova, 35122, Italy*

<sup>4</sup> *International Centre for Radio Astronomy Research, The University of Western Australia, 35 Stirling Highway, Crawley, WA 6009, Australia*

17 October 2021

## ABSTRACT

We present the results of deep high resolution imaging performed with ACS/HRC@HST in the most active region of the nearby starburst galaxy NGC 4214. We resolved the stellar populations of five Young Massive Clusters and their surrounding galactic field. The star formation history of this region is characterized by two main bursts occurred within the last 500 Myr, with the oldest episode spread out across an area larger than that covered by the most recent one. The ages derived for the analysed clusters cover a wide range between  $6.4 < \log t/yr < 8.1$  in agreement with those predicted by recent analyses based on integrated photometry. The comparison between the mass of the young associations and that of the surrounding field population with similar ages indicates a high cluster formation efficiency ( $\Gamma \sim 33\%$ ) which decreases when old populations are considered. The mass function of the major assembly has been found to be slightly flatter than the Salpeter (1955) law with a hint of mass segregation. We found no clear signatures of multiple stellar populations in the two young ( $\log t/yr < 6.8$ ) associations where we were able to resolve their innermost region. The masses and sizes of three clusters indicate that at least one of them could evolve toward a globular cluster-like structure.

**Key words:** methods: data analysis – methods: observational – techniques: photometric – galaxies: individual: NGC 4214 – galaxies: star clusters: general – galaxies: starburst.

## 1 INTRODUCTION

The study of the star formation histories (SFH) of dwarf galaxies and the relation with their population of massive clusters constitutes a crucial piece of information to understand how star formation proceeded in the early stages of formation of structures in the Universe. One of the main cosmological interests is related to the possibility that today's dwarfs are the remnants of the building blocks of massive galaxies. In the context of the widely accepted cosmological model  $\Lambda$ -Cold Dark Matter, more massive systems are assembled by subsequent merging of these protogalactic fragments (the hierarchical formation scenario; e.g., White &

Rees 1978; Frenk et al. 1988). The SFH of dwarfs with different morphological type are quite different (see Tolstoy, Hill & Tosi 2009 for a recent review). In particular, early-type dwarfs have little or no SF in the last few Gyrs (e.g. Weisz et al 2011), whilst all late-type dwarfs experience more recent star formation activities, with major peaks in the last few Gyrs (e.g. Cole et al 2007; Cignoni et al 2013), although many of them appear to have formed the majority of their stellar mass prior to 7.6 Gyr ago (Weisz et al 2011). Among the latter group, starburst galaxies, characterized by a recent intense SF activity, constitute an interesting class of objects. Although they are quite rare in the local Universe, their fraction increases at high redshift (Vieira et al. 2013) indicating a larger frequency of starbursts in the early Universe. As all the starburst galaxies in the nearby Universe are located outside the Local Group, their SFH could be determined only in recent years through Hubble Space Telescope observations (Greggio et al. 1998; Aloisi, Tosi &

<sup>\*</sup> Based on observations made with the NASA/ESA Hubble Space Telescope, which is operated by the association of Universities for Research in Astronomy, Inc., under the NASA contract NAS 5-26555, under program GO-10332 (PI: Ford)

<sup>†</sup> E-mail: antonio.sollima@oabo.inaf.it

Greggio 1999; Silva-Villa & Larsen 2012; García-Benito & Pérez-Montero 2012).

Massive clusters are important tracers of the stellar content of their host galaxy and their study provides crucial insight on the understanding of the star formation process at different epochs. For instance, the correlation of the properties (colours, magnitudes) of old globular clusters (GCs) with those of their host galaxy is a valuable information to understand whether its GC system formed in-situ or was accreted (Larsen et al. 2001). On the other hand, young clusters provide information on the recent star formation activity of galaxies. It has been suggested that up to  $\sim 40\%$  of the stars in galaxies formed in temporary bound systems (Kruijssen 2012) which later dissolve as an effect of the expulsion of residual gas by feedback (Tutukov 1978; Parmentier et al. 2008). Young Massive Clusters (YMCs; with  $\log t/\text{yr} < 8$  and  $\log M/M_\odot > 4$ , Portegies-Zwart, McMillan & Gieles 2010) are among the most interesting objects in this context. They have been observed in the Milky Way and the Local Group galaxies, but their fraction is strikingly high in starburst and interacting galaxies, being tightly correlated with the star formation rate of the host galaxy (Larsen & Richtler 2000; Billett, Hunter & Elmegreen 2002). YMCs trace the recent star forming activity of distant galaxies and may be used to study the star-cluster mass function. On the other hand, the closest YMCs are of prime interest to study the shape and the homogeneity of the stellar mass function in an environment which has still not been affected by dynamical processes like two-body relaxation, and the interplay between stellar evolution and stellar dynamics. Furthermore, they are the best candidates to be the progenitors of GCs, sharing in some cases similar masses and sizes. Their young ages allow therefore to study the early evolution of massive star clusters in the stage when they are expected to form multiple generation of stars (e.g. D’Ercole et al. 2008). While the integrated properties of YMCs have been studied in detail in the past decades (Arp & Sandage 1985; Silva-Villa & Larsen 2011), resolved photometry has been feasible only for Milky Way YMCs (Figer et al. 1999, 2006; Davies et al. 2007) and, only very recently, in nearby galaxies (Perina et al. 2010; Larsen et al. 2011).

NGC 4214 is a nearby dwarf IAB(s)m galaxy (de Vaucouleurs et al. 1991) in the low-redshift CVn I Cloud (Sandage & Bedke 1994) located at a distance of  $3.04 \pm 0.05$  Mpc (Dalcanton et al. 2009). It has a mass of  $M \sim 5 \times 10^9 M_\odot$  (Karachentsev et al. 2004) and a low metal-content ( $-1.6 < [M/H] < 0$ ; Williams et al. 2011 hereafter W11). NGC 4214 is characterized by an intense recent star-formation activity, as shown by the presence of two HII star forming complexes located in its central region (Fanelli et al. 1997). Recently, McQuinn et al. (2010) and W11 used Hubble Space Telescope (HST) photometric observations to study the field population of NGC4214. They found a SFH characterized by an old episode occurred more than 2 Gyr ago followed by an intense recent SF activity. The large majority of the galaxy stellar population ( $\sim 75\%$  of the total galaxy mass) appears to be homogeneously distributed across the galaxy except for the young stellar population which is more centrally concentrated. MacKenty et al. (2000) provided a detailed classification of the  $H\alpha$  knots visible in HST images, identifying 13 relatively bright YMCs. Recently, Úbeda, Maíz-Apellániz & MacKenty et al.

(2007a,b) and Sollima et al. (2013) used imaging from the WFPC2@HST associated to infrared photometry to determine ages, masses and extinction of a sample of YMCs. In both the above studies YMCs cover a wide range in age ( $6.2 < \log t/\text{yr} < 8.3$ ) and masses ( $3.7 < \log M/M_\odot < 6$ ). Dust absorption appears to be on average relatively low ( $E(B-V) < 0.1$ ; W11, Sollima et al. 2013) although patchy with some regions heavily obscured (Maíz-Apellániz 1998; Beck, Turner & Kovo 2000; Úbeda et al. 2007a,b).

In this paper we present the resolved photometry of five young stellar complexes of NGC 4214 obtained using ACS@HST. These data are used to determine ages, masses and half-light radii of these objects and the SFH of their surrounding field. Throughout the paper we use the naming convention for clusters by Ubeda et al. (2007a; see their Fig. 2). The paper is organized as follows: in Sect. 2 we describe the observations and the data reduction technique. In Sect. 3 the obtained colour-magnitude diagrams (CMDs) are presented. In Sect. 4 the SFH of the field population is presented and discussed. Sect. 5 is devoted to the determination of ages, masses and half-light radii of the YMCs and associations of NGC 4214 and to the determination of the mass function and the degree of primordial mass segregation of the resolved association I-A. Finally, we summarize and discuss our results in Sect. 6.

## 2 OBSERVATIONS AND DATA REDUCTION

The analysed dataset consists of a set of images obtained with the High Resolution Channel (HRC) of the Advanced Camera for Survey onboard HST under the program GO-10332. This camera provides a field of view of  $29'' \times 26''$  with a plate scale of  $0.027'' \text{ px}^{-1}$ . Two regions of the main star forming complex 4214-I have been observed through the F330W, F555W and F814W filters: *i*) a pointing centered on the largest association (I-A) and containing also cluster I-Es, and a portion of the association I-B (hereafter referred as *central field*), and *ii*) a pointing centered on cluster IVs which includes also cluster IIIs at the edge of the frame (hereafter *offset field*). The two fields are offset by  $\sim 30''$  ( $\sim 440$  pc at the distance of NGC 4214) with only a marginal overlap. The false colour images of the two pointings are shown in Fig. 1. In the *central field* the two main associations I-A and I-B are evident as two distinct assembly of blue objects immersed in a population of red stars. Two diffuse shells surrounding the two main associations are particularly evident in the F555W image as a consequence of the strong  $H\beta$  and  $[OIII]$  emission of gas. The *offset field* is instead dominated by red stars covering the entire field of view. Three exposures for each filter have been obtained with exposure times of 223, 130 and 120 s in the F330W, F555W and F814W filters, respectively. All images were passed through the CALACS reduction pipeline. Data reduction has been performed on the individual pre-reduced (.flt) images using the DAOPHOT II package (Stetson 1987). For each image an empirical Point Spread Function has been determined using  $\sim 50$  isolated bright stars. Source detection has been performed on the stack of all images while the photometric analysis was performed independently on each image. Only stars detected in at least two out of three long exposures have been included in the final catalog. The final magnitudes

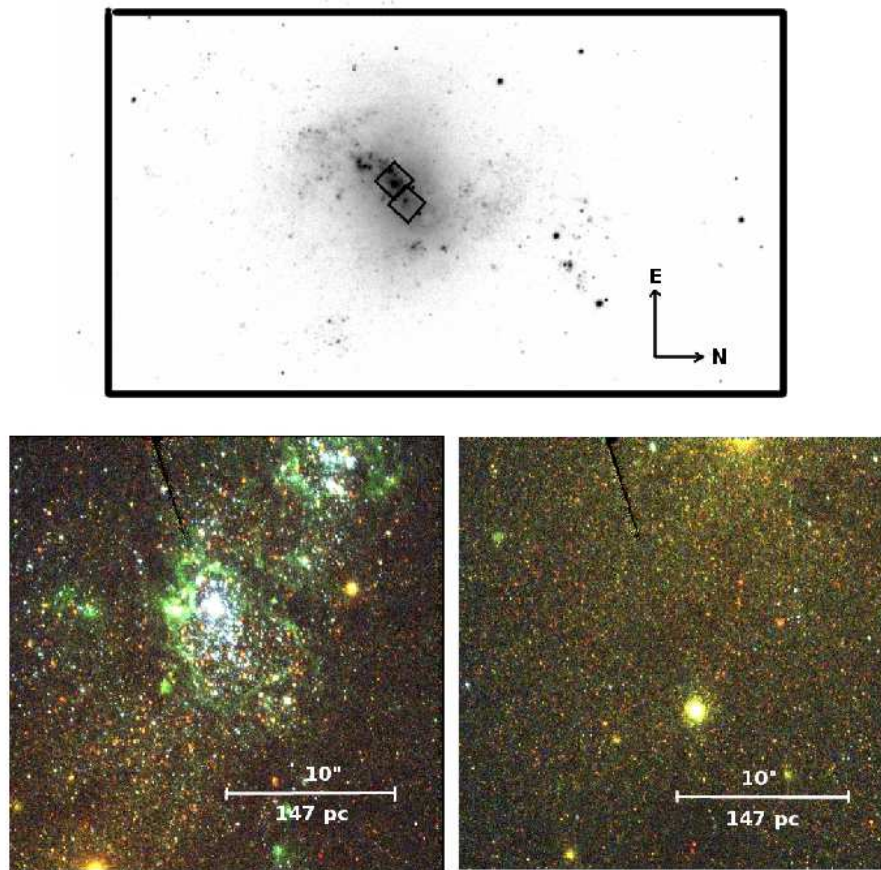


**Figure 1.** Location of the two HRC/ACS pointings on the SDSS  $g$  image of NGC4214 (top panel). In the lower panels the false-colour image of the two HRC pointings of NGC 4214 (left: central field; right: offset field) are shown. The F330W, F555W and F814W images have been combined in the blue, green and red channels, respectively (in the printed version of the paper the F555W band image is shown in greyscale). The angular and physical scale (adopting a distance of 3.04 Mpc) are indicated in both panels.

have been obtained as the average of single exposure measures and the related r.m.s. has been assigned as their error. We used the most isolated and brightest stars in the field to link the aperture magnitudes at 0.5 arcsec to the instrumental ones, after normalizing for exposure time. Instrumental magnitudes have been then transformed into the VEGA-MAG system using the photometric zero points by Sirianni et al. (2005). Our photometry has been compared with the catalog by Ubeda et al. (2007a) obtained from WFPC2 data in the F336W and F555W filters. The mean magnitude differences are  $F_{336W_{WFPC2}} - F_{330W_{HRC}} = -0.20 \pm 0.05$  and  $F_{555W_{WFPC2}} - F_{555W_{HRC}} = -0.05 \pm 0.03$ . The above differences can be entirely addressed to the different filters adopted by these authors (see Sirianni et al. 2005).

We performed artificial star experiments on the science frames: a set of artificial stars have been simulated using the same PSF model extracted in the science frames and added to all images at random positions within  $24 \times 24$  pixel cells centered on a grid of  $20 \times 20$  positions along the  $x$  and  $y$  directions of the chip (a single star for each cell). The magnitudes of the artificial stars have been assigned following a homogeneous distribution in F555W magnitude and (F330W-F555W) and (F555W-F814W) colours within the ranges  $18.5 < F_{555W} < 26.5$ ,  $-2 < (F_{330W} - F_{555W}) < 1$

and  $-1 < (F_{555W} - F_{814W}) < 3$ . We performed the photometric reduction on the simulated frames with the same procedure adopted for the science frames producing a catalog of  $\sim 200,000$  artificial stars which has been used to determine the level of completeness and photometric errors in different positions of the frame.

### 3 COLOUR-MAGNITUDE DIAGRAMS

In Fig. 2 the CMDs of the two observed fields are shown in the F814W vs. (F555W-F814W) and F330W vs. (F330W-F555W) planes. The two diagrams sample the evolved population of NGC 4214 down to  $F_{555W} \sim 26$ , just above the tip of the Red Giant Branch (see W11). The optical CMDs of the two fields appear significantly different from each other. In fact, in the *central field* the prominent blue plume (BP), populated by massive ( $M > 10 M_{\odot}$ ) main sequence (MS) stars and blue Helium-burning (HeB) stars in the range  $6 < M < 16 M_{\odot}$ , is well visible in the blue region of the CMD at  $(F_{555W} - F_{814W}) < 1$ . At red colours, the population of Red Supergiants (RSG; mainly red intermediate to massive HeB stars), form a well defined sequence at  $(F_{555W} - F_{814W}) > 1$  and  $F_{814W} < 21.5$ . At fainter magnitudes, the red part of this CMD is populated

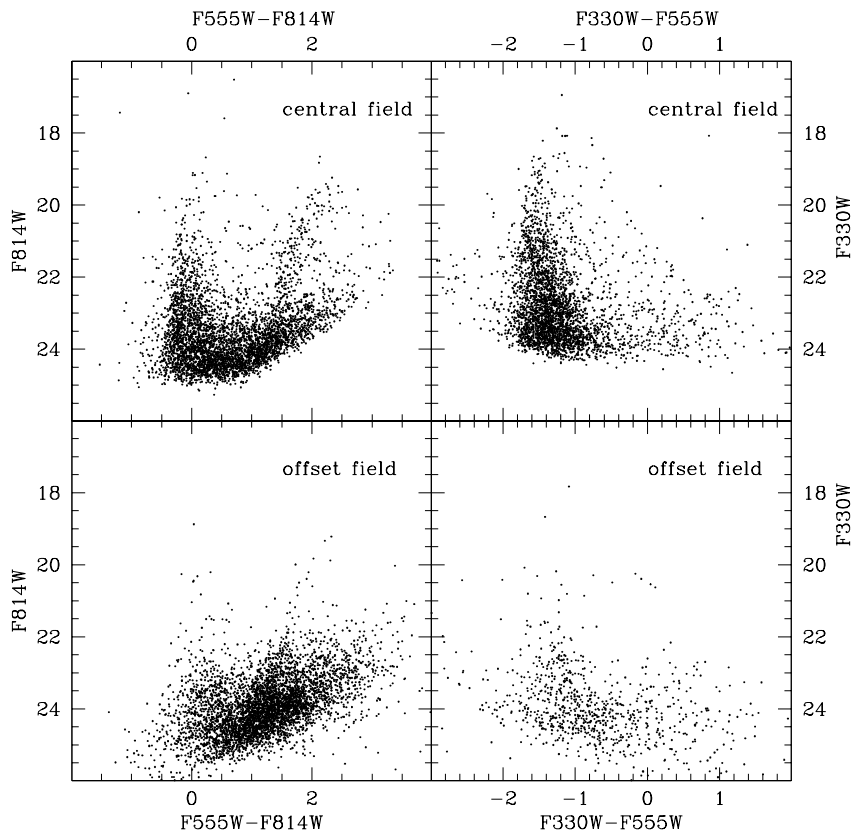


**Figure 2.** CMDs of the two ACS pointings of NGC 4214 (top: *central field*; bottom: *offset field*). Left panels show the F814W vs. (F555W-F814W) CMDs, right panels show the (F330W-F555W) vs. F330W CMDs.

by a significant fraction of intermediate mass ( $M \sim 3 M_{\odot}$ ) Asymptotic Giant Branch (AGB) stars. In the optical CMD of the *offset field* the fraction of both Blue and Red Supergiants is significantly smaller than in the *central field*: only a bunch of blue MS/HeB stars is visible, while the RSG sequence still populates the bright red portion of the CMD.

In the F330W vs. (F330W-F555W) CMDs most of the stars are intermediate to massive MS objects with color around -1.5, while the few objects at the right of the MS are likely HeB stars. It is apparent that the recent star formation (SF) activity of the *central field* is more intense than that in the *offset field*.

## 4 THE FIELD POPULATION

### 4.1 Star Formation History

We use the CMDs shown in Fig. 2 to determine the star formation history (SFH) of the field population surrounding the YMCs and associations in the two observed regions. We adopted the synthetic CMD method already applied in many recent works (see e.g. Cignoni et al. 2012 and references therein). The CMDs of the two observed fields have been compared with a library of synthetic CMDs computed with different values of metallicity, ages, and reddening. The synthetic CMDs have been calculated using evolutionary tracks

by Marigo et al. (2008) for masses between the hydrogen-burning limit (at  $0.1 M_{\odot}$ ) and  $100 M_{\odot}$ . Theoretical temperature and luminosity have been transformed into the observational plane in the ACS/HRC VEGAMAG photometric system using the transformations by Girardi et al. (2008).

The recipe to build a "synthetic" CMD is the following. Using a Monte Carlo algorithm, masses and ages are extracted according to the initial mass function (IMF) and the SF law. The extracted synthetic stars are placed in the CMD by interpolation among the adopted stellar evolution library. The synthetic population is put at the distance of the region we want to analyse, simultaneously correcting for reddening and extinction. Then, to each synthetic star an artificial star with similar colours and magnitude is associated (see Sect. 2), and its output-input magnitudes differences are added to the magnitudes of the synthetic star. This last step simultaneously accounts for photometric errors, incompleteness and blending.

In order to reduce the computational time, a generic SFH is built up from a linear combination of simple synthetic stellar populations. The Star Formation Rate (SFR) is parameterized as a linear combination of chosen basis CMDs, where each basis is a Monte Carlo extraction from a step star formation episode. The basis CMDs are constructed with all the metallicities available in the adopted stellar library. No metallicity is assumed a priori.

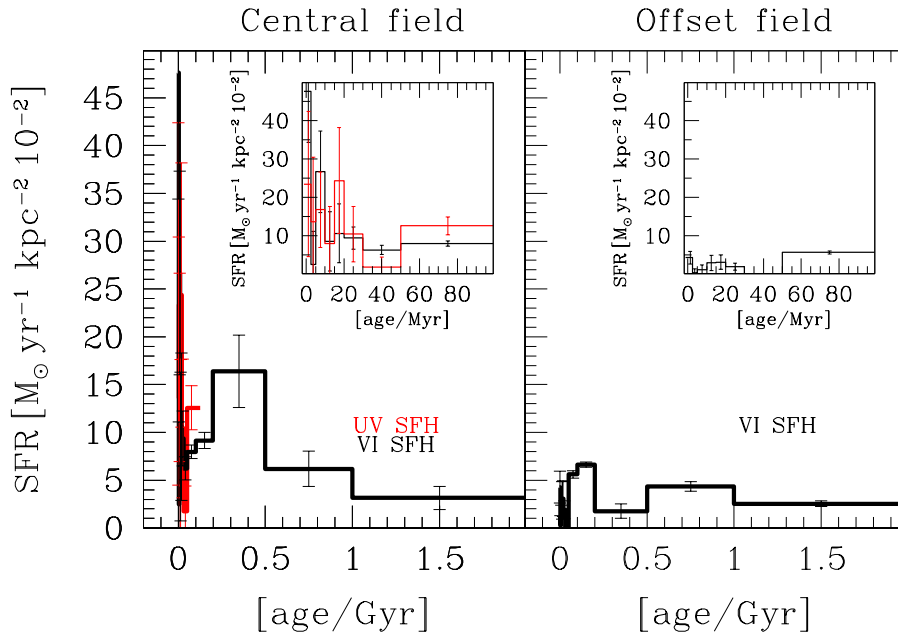


**Figure 3.** SFH derived for the *central field* (left panel) and the *offset field* (right panel). The black histograms show the SFH derived from the F555W vs. (F555W-F814W) CMDs, the red histograms (grey in the printed version of the paper) in the left panel show the SFH derived from the F555W vs. (F330W-F555W) CMD. The inner boxes show a zoom in of the first 100 Myr.

Within the framework of the adopted stellar tracks and atmosphere models, we chose as the most likely SFH the one which minimizes the differences between data and synthetic star counts over CMD boxes 0.1 mag wide in the V band and 0.05 mag wide in colour. The degree of likelihood is assessed through a  $\chi^2$  minimization and a downhill simplex algorithm. In order to escape from local minima, the simplex is re-started from thousands of initial random positions and a temperature parameter is implemented. A bootstrap method is used to assess the effect of random errors. The search of the best SFH is repeated for each bootstrapped data set, producing a distribution of best solutions. The error bars on the final SFH represent one standard deviation using 100 bootstraps.

The SFH of the *central field* has been recovered both for the F555W vs. (F555W-F814W) and the F555W vs. (F330W-F555W) CMDs independently while for the *offset field* (dominated by red stars; see Sect. 3) only the F555W vs. (F555W-F814W) CMD has been used.

We excluded from the analysis the regions containing the known YMCs and associations up to the distance where the star density is equal to that of the surrounding population (see Sect. 5.1). We adopted a fixed distance modulus of  $(m - M)_0 = 27.41$  (Dalcanton et al. 2009) and the IMF of Kroupa (2001). Although recent works suggest the occurrence of significant variations of the IMF shape in different galaxy types (Hoversten & Glazebrook 2008; Meurer et al. 2009; Lee et al. 2009; Gunawardhana et al. 2011), the analysis of this effect is beyond the aim of our work, so we keep the IMF shape fixed. As the distribution of dust in NGC 4214 has been found to be patchy (Úbeda et al. 2007b), we considered the possibility of differential reddening across

the field. For this purpose, we adopt a gaussian distribution of  $E(B-V)$  with central value and dispersion chosen to best reproduce the location of bright ( $F555W < 22$ ) stars in the (F330W-F555W) vs. (F555W-F814W) colour-colour diagram. In this magnitude range only very young stars ( $t < 10$  Myr) are present, so the age-reddening degeneracy is minimized. The best fit reddening for the *central field* turns out to be centered at  $E(B-V)=0.2$  with a standard deviation  $\sigma_{E(B-V)} = 0.1$ . Instead, the *offset field* appears to be characterized by a single low value of  $E(B-V)=0.05$ , which is compatible with the foreground reddening predicted by Schlegel, Finkbeiner & Davis (1996) maps.

Assuming these reddening values, we searched for the best fitting SFH by changing the metallicity. We found that  $Z=0.008$  is the best compromise to reproduce at the same time the BP and the RSG sequence: higher metallicities tend to split the BP into two separate sequences (MS and blue HeB stars), while lower values tend to produce a too blue RSG sequence. This value is compatible with the range of metallicities ( $-0.5 < [M/H] < 0$ ) found by W11 by fitting the young population and is slightly higher than that found by Kobulnicky & Skillman (1996) using nebular abundances ( $[O/H] \sim -0.5$ ). Fig. 3 shows the derived SFH for the two fields, while Figs. 4 and 5 show the observed and the best fit synthetic CMDs respectively.

The observational and synthetic CMDs agree with each other. In the central field the BP is well matched in both the F555W vs. (F330W-F555W) and F555W vs. (F555W-F814W) planes, except above  $F555W = 20$ , where both the synthetic CMDs are less populated than the observational ones. Some differences appear also in the RSG phase. In the F555W vs. (F555W-F814W) plane the upper part

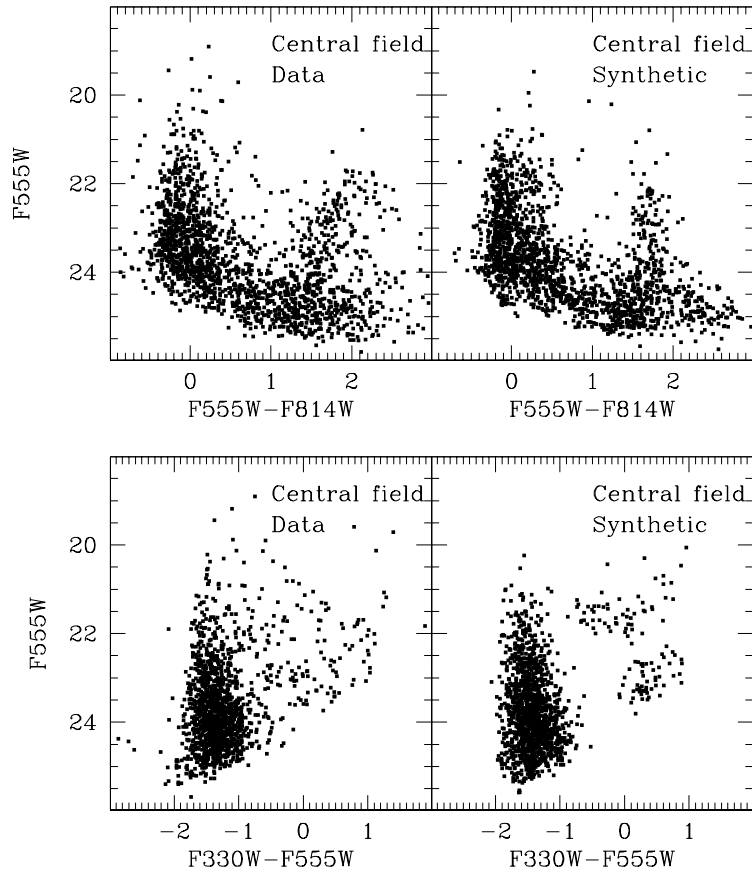


**Figure 4.** Comparison between the observed (left panels) and synthetic (right panels) CMDs of the *central field*. Top panels show the F555W vs. (F555W-F814W) CMD, bottom panels show the F555W vs. (F330W-F555W) CMD.

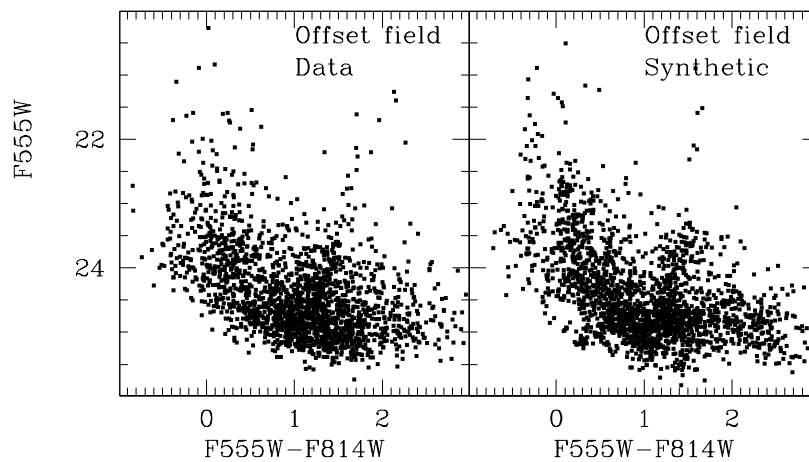


**Figure 5.** Same of Fig.4 but for the *offset field*. Only the F555W vs. (F555W-F814W) CMD has been used for this field to derive the SFH.

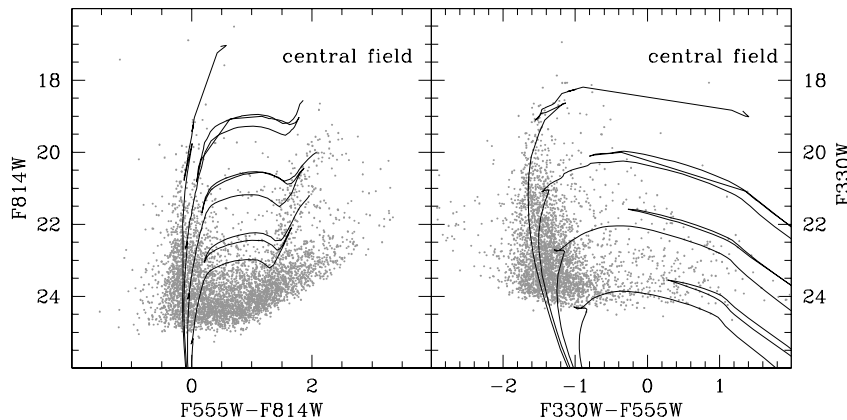


**Figure 6.** CMDs of the *central field*. The left panel shows the F814W vs. (F555W-F814W) CMD, the right panel shows the F330W vs. (F330W-F555W) CMD. A set of Marigo et al. (2008) isochrones with  $Z=0.008$  and  $\log t/\text{yr}=6.6, 7, 7.4$  and  $7.8$  are overplotted in both panels.

of the synthetic RSG is bluer and shorter, thus suggesting that the red edge of the blue loop phase in the model is too blue. On the other hand, in the F555W vs. (F330W-F555W) plane our best model produces a clear sequence of HeB stars (HeB stars at the blue edge of the blue loop), while the observed distribution is smooth. This continuity between MS and HeB stars is puzzling, since Marigo et al. (2008) isochrones (see Fig. 6) predict a clear gap (the so-called Blue Hertzsprung gap, which is predicted by many models; see e.g. Chiosi 1998) between the blue edge of the HeB and the MS. This would imply that the stellar models predict longer blue loops at these metallicities, a circumstance that could be favored e.g. by a significant overshooting from convective envelopes (Bressan, private communication).

In the offset field the agreement is generally better. Our synthetic BP and RSG sequences reproduce well star counts and morphologies of the observational counterparts although a mild colour split along the synthetic BP and a slightly larger ratio of HeB/RSG stars are visible.

We interpret the differences between observational and theoretical CMDs as being, at least in part, an effect of the adopted stellar tracks. A likely explanation for the lack of bright BP stars in the models is that several BP stars are not MS stars but actually intermediate/massive HeB stars, which are predicted to be too red in our model. Indeed, the synthetic F555W vs. (F330W-F555W) CMD shows a clear separation between MS and HeB stars, which is not seen in the observations. A similar discrepancy is also found by Larsen et al. (2011) in YMCs. Although a lower metallicity could alleviate this issue, increasing the excursion to the blue of the HeB stars, it would also produce a bluer RSG in the optical CMD, thus exacerbating the difference between data and model in the red. Alternative explanations could be the rate of mass loss and rotation. Indeed, stronger mass loss during the RSG phase could favour a bluewards evolution (see e.g. Salasnich, Bressan & Chiosi 1999) and, in turn, a higher ratio between blue and red supergiants.

Moreover, when rotation is taken into account, a large fraction of the end of the core HeB phase is spent in the blue. In this respect, the new rotating models of Ekström et al. (2012) predict that the ratio between blue and red lifetime for a  $20 M_{\odot}$  model could be up to 7.5 times higher than for the not-rotating models of Schaller et al. (1992). A possible solution could result from the inclusion of significant overshooting from convective envelopes in the stellar models (Bressan, private communication). We then think that stellar models are the major source of discrepancy.

Because of the relatively bright limiting magnitude of our catalog, we were able to derive the SFH only to few Gyr in lookback time. The *central field* appears to be characterized by a double peaked SFH with a prominent episode of SF at  $t \sim 300$  Myr and another recent intense episode of SF at  $t \sim 8$  Myr. The SFH derived on the basis of the F555W vs. (F555W-F814W) and the F555W vs. (F330W-F555W) CMDs agree with each other. Of course, because of the low sensitivity of the ultraviolet filter F330W to the old red populations, the SFH derived using the ultraviolet CMD is truncated at a more recent lookback time.

The *offset field* shows an almost constant SF rate in the last few Gyr. Recently, McQuinn et al. (2010) and W11 derived the SFH of different regions of NGC 4214 using deeper HST data, although with worse spatial resolution. The SFH derived by McQuinn et al. (2010) is characterized by two major epochs of enhancement. The older episode took place  $\sim 3$  Gyr ago and produced most of the stars, the recent one started 1 Gyr ago and is now at its highest level. A similar behaviour has been found by W11 in their inner field (covering a wide area of  $\sim 123'' \times 136''$  around the galaxy center), although the older episode has been estimated at more remote epochs ( $\sim 8$  Gyr). Compared to our solution, intermediate age and recent rates agree well. In particular, we also predict a low-activity period until 1 Gyr ago, followed by a growing activity up to now. There are differences in the positions of the secondary peaks, but it is not surprising since our observations allow a higher resolution and cover the in-

nermost portion of the NGC 4214 active region where the recent episodes of SF have occurred. Concerning the early activity, the limiting magnitude of our observations prevents us from reaching populations older than few Gyr, therefore missing the signature of the prominent “old” population detected by W11. Finally, the SFH derived in this work for the old ( $> 200 Myr$ ) stellar population is completely reliant on AGB stars. The modelling of this evolutionary phase is largely uncertain and can produce significant shifts in the derived ages (Melbourne et al. 2012).

## 4.2 Spatial distribution

The SFHs derived in Sect. 4.1 show a clear distinction between a recent ( $\log t/yr < 7$ ) episode and an older ( $\log t/yr > 7.5$ ) one. To study the spatial distribution of the two episodes of SF we adopted the matched filter technique (Rockosi et al. 2002). Briefly, for each observed field the best fit synthetic F555W vs. (F555W-F814W) CMD has been split in two samples according to the star ages ( $\log t/yr \leq 7.3$ ). To each observed star, a weight proportional to the ratio of densities in the CMD of stars belonging to the young/old synthetic populations, calculated at the observed star location, has been assigned. The above procedure allows us to highlight the young (old) population by putting the density of young (old) stars at the numerator of the density ratio. To evaluate the star density in the CMD, we adopted a metric based on the Euclidean distance of each star from the F555W and F814W magnitudes of its neighbor and calculated the density on the basis of the distance of the 5th nearest star. The final density map in the x,y plane has been then calculated by using a fixed gaussian kernel estimator (Silverman 1986) where the volume of each component has been assigned proportionally to the star weight. The obtained spatial distribution of the young and old populations in the two observed fields are shown in Fig. 7. A clear correlation is apparent between the location of the young/old objects with that of the corresponding field populations. In particular, the two major associations I-A and I-B dominate the young population of the *central field*, with a possible evidence of a bridge of stars connecting these two major associations. Other assemblies of young stars are also evident across the field of view. The old population appears to be segregated from the young component, populating mainly the bottom part of the field of view close to the location of the (relatively old; see Sect. 5.1) cluster IIIs. A notable exception to such a correlation is represented by cluster I-Es: despite its relatively old age (see Sect. 5.1), it is located close to the young field population. In the *offset field* the young population is almost entirely located in a large scale diffuse region in the upper part of the field of view while the old population mainly surrounds the two older YMCs present in the field.

## 5 YOUNG MASSIVE CLUSTERS

### 5.1 Ages

The superb resolution of the HRC allows one to resolve individual stars in the two major associations (I-A and I-B)

**Table 1.** Adopted apertures and derived parameters of YMCs and associations in

cluster	$R_{ap}$ "	$\log t/yr$	$\log M/M_{\odot}$	$r_h$ "	$r_h$ pc
I-A	2.700	6.4 ( $\pm 0.1$ )	5.02 ( $\pm 0.21$ )	1.58 ( $\pm 0.12$ )	23.2 ( $\pm 2.0$ )
I-B	2.160	6.8 ( $\pm 0.1$ )	– –	– –	– –
I-Es	0.675	7.7 ( $\pm 0.3$ )	4.45 ( $\pm 0.32$ )	0.15 ( $\pm 0.01$ )	2.25 ( $\pm 0.15$ )
IIIs	1.620	8.1 ( $\pm 0.1$ )	– –	– –	– –
IVs	1.080	8.0 ( $\pm 0.1$ )	5.11 ( $\pm 0.33$ )	0.23 ( $\pm 0.02$ )	3.43 ( $\pm 0.35$ )

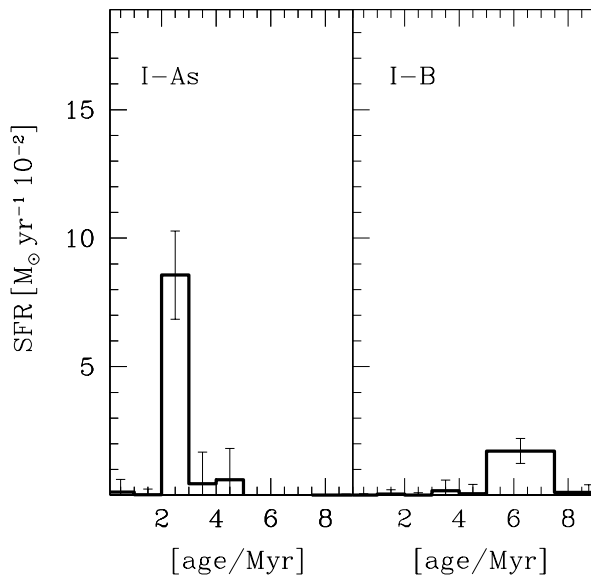


**Figure 8.** SFH derived for associations I-A (left panel) and I-B (right panel).

and to partially resolve the outskirts of the other three analysed clusters (I-Es, IIIs and IVs). This allows a precise age dating of these clusters as well as an estimate of their sizes and masses. The ages of the two resolved associations have been derived adopting the same technique described in Sect. 4.1. We considered in our analysis only (real and artificial) stars within a radius corresponding to the distance from the cluster center of the locus where the stellar density reaches the level of the background field. According to this definition, a number of field contaminants could be present within the aperture. Since the artificial stars have been distributed uniformly across the field, the estimated completeness and blending fractions represent an average within the adopted aperture. In principle, the different distribution of real and artificial stars could cause an overestimation of the completeness level and an underestimate of the blending fraction with some consequent bias in the SFH and mass determination for this stellar system. However, this affects almost exclusively the faint part of the completeness curve, while



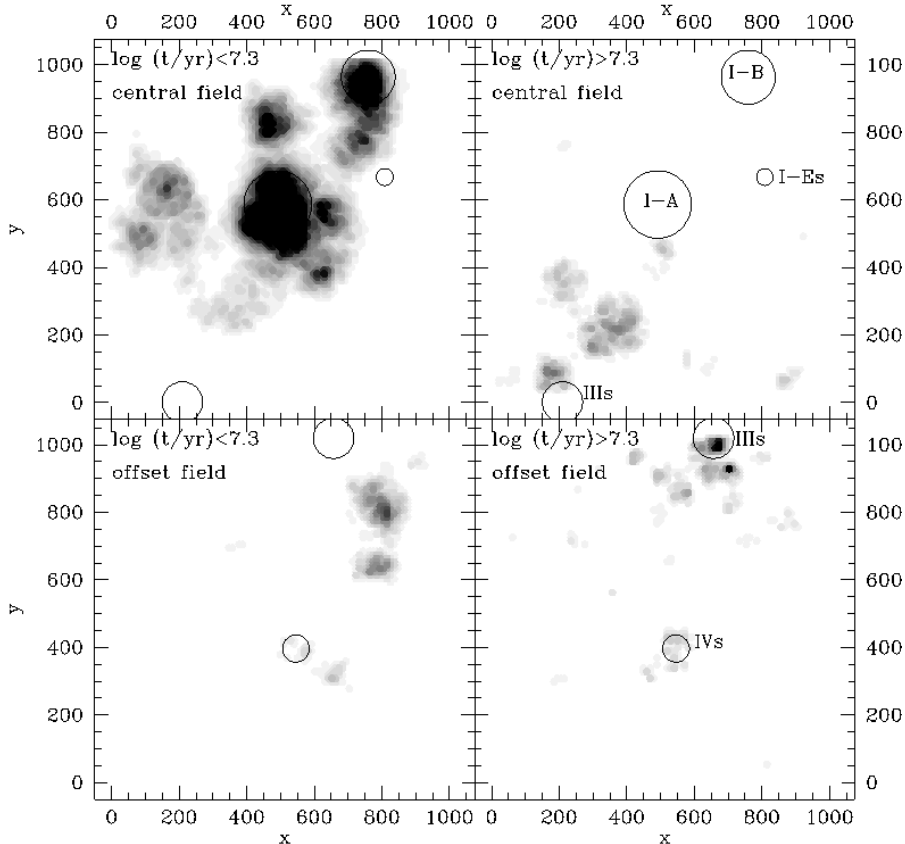


**Figure 7.** Spatial distribution of the young ( $\log t/\text{yr} < 7.3$ ; left panels) and old ( $\log t/\text{yr} > 7.3$ ; right panels) populations in the two observed fields of NGC 4214. Top panels refers to the *central field*, bottom panels to the *offset field*. The locations of YMCs and associations are marked with open circles. Density contours range from 3 to 10 times density standard deviations above the background level.

bright ( $F555W < 22$ ) stars are almost always recovered even in the most crowded region of the cluster. Since the age determination in young stellar populations, like those of associations I-A and I-B, is mainly driven by the bright stars (at  $F555W < 21$ , where the completeness is  $\sim 90\%$ ), no significant bias is expected to affect our determinations. To test this last conclusion, for both associations, we repeated the analysis in two regions at different distances to the cluster center ( $\leq 0.5 R_{ap}$ ). As expected, the bestfit ages for both clusters remain unchanged regardless of the considered radial sample. The derived SFHs of both objects are shown in Fig. 8 and the corresponding observed and synthetic CMDs are plotted in Fig. 9. The adopted aperture radii ( $R_{ap}$ ) for the five clusters as well as their derived parameters are listed in Table 1. It is apparent that both associations are characterized by a single prominent peak with a small residual older population. The oldest stars (noticeable in the  $F555W$  vs.  $(F555W-F814W)$  CMD as a sequence of RSG) are homogeneously distributed within the aperture, at variance with the blue MS stars. Both the age and the density of these older stars agree with those of the surrounding field population. Both associations appear to be very young ( $\log t/\text{yr} < 7$ ) in agreement with previous studies (Úbeda et al. 2007b; Sollima et al. 2013; Andrews et al. 2013). No

signs of multiple stellar populations are noticeable in either objects.

A bunch of very bright objects ( $F555W < 20$ ), not reproduced by the synthetic CMDs, can be noticed in both systems. The location of these stars in the CMD is not compatible with any stellar track with  $M < 100 M_{\odot}$ . The fraction of these objects in the field is significantly smaller (see Sect. 4.1). It is therefore likely that they arise from multiple blends of bright stars which are favored by the extreme crowding conditions met in clusters.

For the other three clusters only a small number of stars in their peripheral region have been resolved. In these cases, the CMD synthesis technique cannot be applied. To determine the age of these YMCs we compare the location of observed stars with the density of stars predicted by synthetic CMDs, after correcting for field contamination. For this purpose we adopted the following procedure:

- We simulated a single episode of SF with a large ( $> 10^6$ ) number of stars using the stellar models and the prescription on IMF, metallicity, reddening and distance reported in Sect. 4.1 and different ages. The synthetic CMD has been corrected for completeness and photometric errors using the set of artificial stars described in Sect. 2.

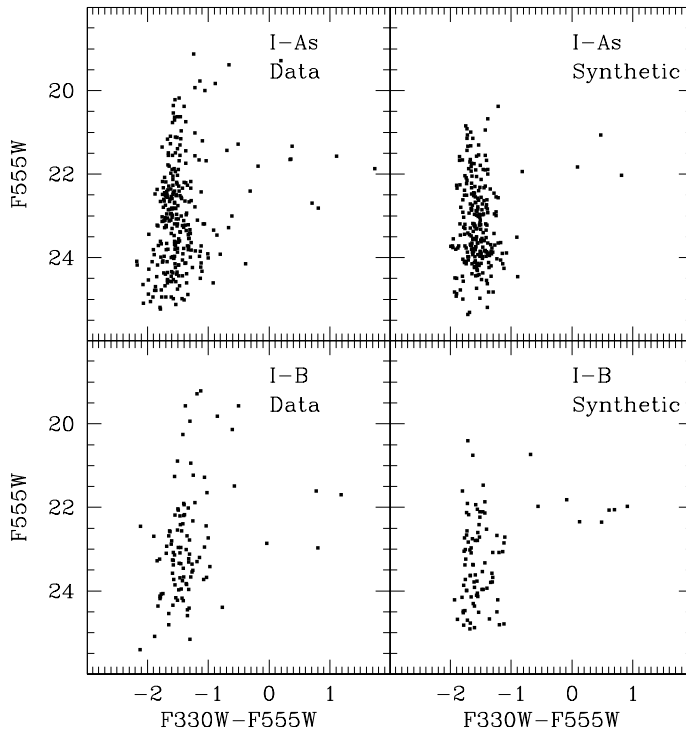


**Figure 9.** Comparison between the observed (left panels) and synthetic (right panels) F555W vs. (F330W-F555W) CMDs of associations I-A (top panels) and I-B (bottom panels).

- We selected the CMD of the reference field population extracted in an annulus covering  $\sim 4$  times the cluster area.

- We calculated the density of stars belonging to the cluster catalog ( $\rho_{cl}$ ), the field catalog ( $\rho_{field}$ ) and the synthetic catalog ( $\rho_{synth}$ ) at the position of each observed object in the F814W vs. (F555W-F814W) CMD. For this purpose, we adopted a metric based on the Euclidean distance of each synthetic star from the observed F555W and F814W magnitudes and calculated the density on the basis of the distance of the 5th nearest star. The density of field stars has been normalized to the ratio of the field and cluster areas.

- We calculated the merit function

$$L = \frac{\sum_{i=1}^{N_{cl}} w_i \rho_{synth}}{N_{synth}}$$

where  $N_{cl}$  and  $N_{synth}$  are the number of stars in the observed and synthetic catalog and

$$w_i = 1 - \rho_{field}/\rho_{cl}$$

is a weight proportional to the probability of a star to be a cluster member, on the basis of the ratio of densities of field and cluster in the CMD.

The above procedure has been repeated adopting various ages and the value maximizing the above defined merit function has been selected as the best fit. To evaluate errors on the derived ages, the above procedure has been repeated 100 times by replacing the observed catalog with other realizations of synthetic CMDs with the same number of stars  $N_{cl}$ . The standard deviations of the derived ages has been

assumed as the formal  $1 \sigma$  errors. In Fig. 10 the F555W vs. (F555W-F814W) CMD of these three clusters are compared with the Hess diagrams of the best fit synthetic populations. It is noticeable that these three YMCs are all significantly older than the two major associations (with ages  $\log t/yr > 7.5$ ), although the sparse number of stars in cluster I-Es makes this age estimate largely uncertain. In Fig. 11 the ages derived here are compared with those estimated by Úbeda et al. (2007b) and Sollima et al. (2013) on the basis of their integrated photometry. The agreement is good, without significant offsets and a r.m.s. of  $\sigma_{\log t/yr} = 0.75$  (with respect to Úbeda et al. 2007b) and  $\sigma_{\log t/yr} = 0.39$  (with respect to Sollima et al. 2013), compatible with the combined errors of both studies. In this regard, it is interesting to note that for the three YMCs with multiple age solutions in Úbeda et al. (2007b) (I-Es, IIIs and IVs) our resolved photometry favors the older solution. Andrews et al. (2013) provided ages for the young associations of NGC 4214 obtaining for I-A and I-B ages of  $4.2 \pm 1.6$  and  $2.6 \pm 0.5$  Myr ( $4.8$  Myr for both clusters adopting different SED prescriptions), respectively. The ages estimated by these authors are generally similar to those found in this paper, and the small differences are likely due to the different models and the lower reddening adopted by these authors.

## 5.2 Half-light radii

Another important information we can derive from our photometry are the half-light radii of the observed stellar com-

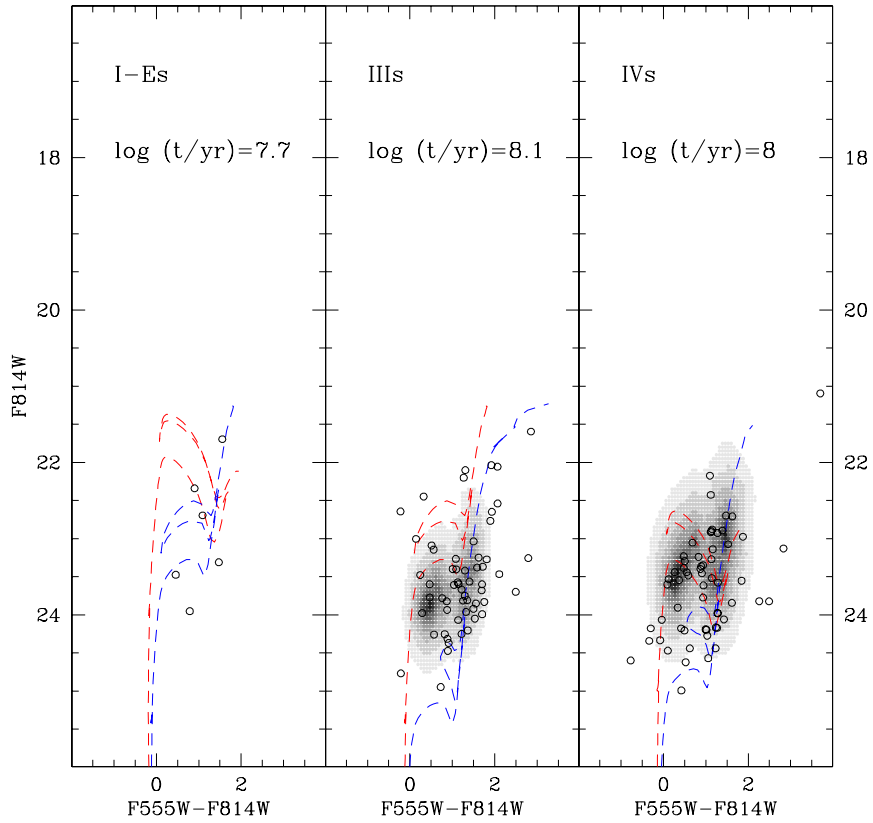


**Figure 10.** Comparison between the observed F814W vs. (F555W-F814W) CMDs of the few resolved stars (open circles) of the clusters I-Es, IIIs, and IVs and the best fit synthetic models. The isochrones with ages  $\Delta \log t/\text{yr} \pm 0.2$  with respect to the best fit models are marked with dashed lines. For clusters IIIs and IVs the Hess diagrams of the best fit models are shown.

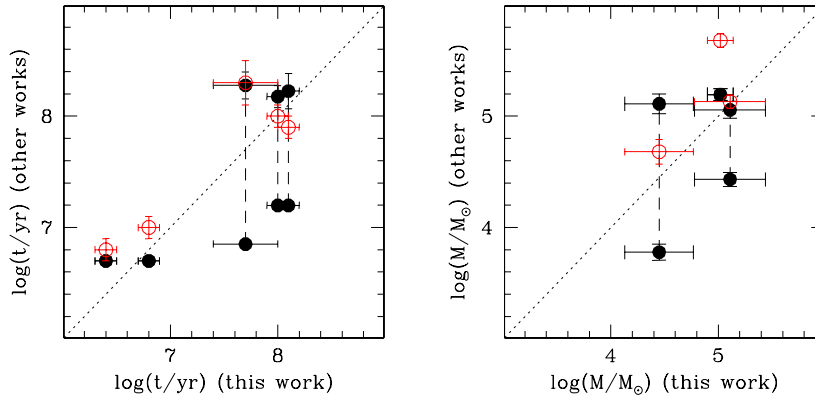


**Figure 11.** Comparison between the ages (left panel) and masses (right panel) derived in this work with those by Úbeda et al. (2007b; black dots) and Sollima et al. (2013; open dots). Dashed lines indicate the range covered by the multiple solutions found by Úbeda et al. (2007b). Dotted lines mark the one-to-one relation.

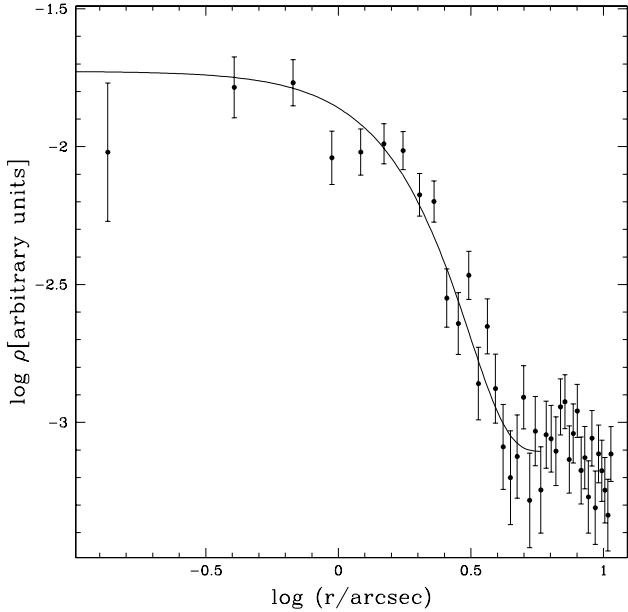


**Figure 12.** Number density profile of association I-A. The best fit King (1966) model is overplotted.

plexes. For the association I-A, where we could resolve the innermost region, this has been done by counting the number of stars in concentric annuli, correcting their number for the local completeness level and dividing by the annulus area. Unfortunately, the center of association I-B lies outside the edge of the detector in the *central field*, so we could not determine its radial profile. The center of association I-A has been derived through an iterative procedure in which at each iteration the  $x$  and  $y$  coordinates of stars within circles of 100 px radius were averaged and the resulting mean value was then adopted in the next iteration as the candidate center. We selected only stars brighter than  $F555W < 22$  (where the completeness level is  $\sim 50\%$  in the innermost region) to avoid large completeness corrections. The radial density profile of association I-A is shown in Fig. 12. A King (1966) model has been fitted to the obtained profile to estimate the object half-light radius.

For the marginally resolved clusters we determined their half-light radii by bestfitting the 2D  $F555W$  flux distribution with a set of King (1962) models convolved with the HRC Point Spread Function (Krist, Hook & Støher 2010). For this purpose we used ISHAPE (Larsen 1999), a specially designed software to derive the structural parameters of slightly resolved astronomical objects. With this procedure we were able to derive the half-light radii of clusters I-Es and IVs, while cluster IIIs (located at the edge of the detector field of view) has been excluded from the analysis.

The half-light radii of the three analysed stellar systems are reported in Table 1.

### 5.3 Masses

Masses have been determined for the stellar systems entirely sampled in the two pointings (I-A, I-Es and IVs). For the association I-A, where we could apply the CMD synthesis

technique, the mass is constrained by matching the number of observed stars. As the different radial distribution of artificial and real stars could produce significant bias in the completeness estimate at faint magnitudes (see Sect. 5.1), we corrected the observed number of stars in the bright portion of the CMD (at  $F330W < 22.4$ ) adopting a local completeness estimate: the completeness factor of each star has been estimated using the artificial stars with distance from the cluster center and magnitudes within 10 px and 0.25 mag from those of the considered star. The contribution of the field population has been estimated in an annulus surrounding the cluster and removed. Moreover, since the limiting magnitude of our photometry samples only relatively massive ( $M > 3 M_{\odot}$ ) stars, an extrapolation has been done at lower masses assuming a Kroupa (2001) IMF. For the other two clusters (I-Es and IVs) masses have been determined from their integrated  $F555W$  magnitude. For this purpose, we used the PHOT task of the DAOPHOT package (Stetson 1987). We chose a large aperture covering the entire cluster extension and a surrounding annulus to subtract the background<sup>1</sup>.  $F555W$  luminosities have been therefore transformed into masses by adopting the  $M/L_{F555W}$  ratio appropriate for their best fit age (calculated by folding the selected isochrone with a Kroupa 2001 IMF). For these two older clusters a mass contribution from white dwarfs has been added assuming the initial-final mass relation by Kruijssen (2009). The use of the integrated magnitude to estimate the clusters' masses could lead to potentially important biases linked to the uncertainties of  $M/L_{F555W}$  ratios and the stochastic errors due to the contribution of few bright stars (Fouesneau et al. 2010; Popescu & Hanson 2010). Note however that the magnitude of stochastic effects drastically decreases at ages  $\log t/yr > 8$  and masses  $\log M/M_{\odot} > 4$  (Beerman et al. 2012). For the typical ages and masses of our targets this translates into a systematic uncertainty of  $\sigma_{\log M/M_{\odot}} \sim 0.2 - 0.3$ . The obtained masses are reported in Table 1. A comparison with the masses estimated by Úbeda et al. 2007b) and Sollima et al. (2013) is shown in the right panel of Fig. 11. Also in this case, there is a good agreement between all measures without any systematical difference and a r.m.s. of  $\sigma_{\log M/M_{\odot}} = 0.47$  (with respect to Úbeda et al. 2007b) and  $\sigma_{\log M/M_{\odot}} = 0.49$  (with respect to Sollima et al. 2013), compatible with the combined uncertainties of those works. To classify the above objects according to the definition proposed by Billet et al. (2002), we need to convert their unit (integrated  $M_V$  magnitudes at 10 Myr) into solar masses. By adopting the stellar models, metallicity and IMF reported in Sect. 4.1, we derived a limiting mass for a super star cluster of  $\log M/M_{\odot} > 4.5$  and  $4.1 < \log M/M_{\odot} < 4.5$  for a populous cluster. According to this criterion, clusters I-A and IVs can be classified as super star clusters, while cluster I-Es as a populous cluster. The same classification has been given by Billet et al. (2002) for clusters I-Es and IVs, while the association I-A was not included in their sample.

In Fig. 13 the location of the three YMCs in the mass

<sup>1</sup> To properly estimate the background we calculated the mean of the sky pixel (instead of the mode commonly adopted by the PHOT/DAOPHOT algorithm) to account also for the contribution of the resolved background stars.

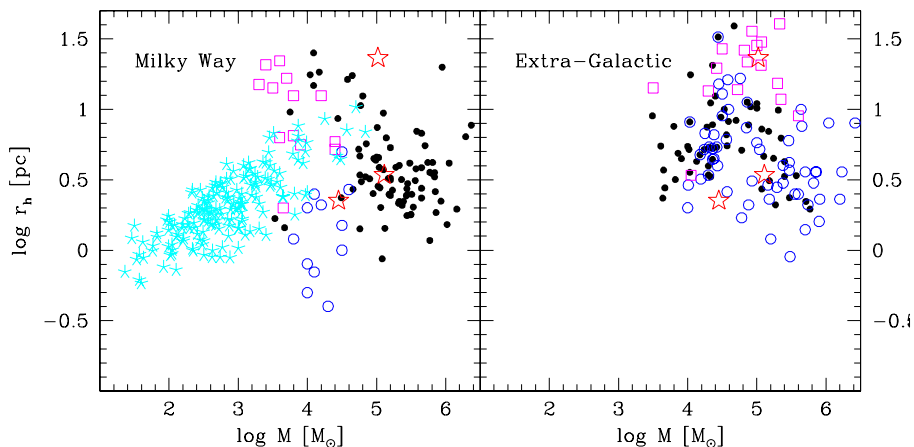


**Figure 13.** Mass vs. half-light radius plane for open clusters (cyan asterisks), compact YMCs (blue open dots), associations (magenta squares) and GCs (black filled dots). The left panel refers to Milky Way objects, the right panel refers to extra-Galactic objects. The location of the three YMCs of NGC 4214 for which masses and half-light radii have been estimated here are marked in both panels with red open stars symbols.

vs. half-light radius plane is compared with those of YMCs, associations (from Portegies-Zwart et al. 2010), open clusters (from Piskunov et al. 2007) and GCs (from McLaughlin & van der Marel 2005) of the Milky Way and other galaxies. The distinction between YMCs and associations has been made on the basis of the ratio between age and dynamical time ( $t_{age}/t_{dyn} \leq 3$ ; Portegies-Zwart et al. 2010). While I-A clearly falls in the region where most extra-Galactic associations are located (in agreement with its ratio  $t_{age}/t_{dyn} = 0.15$ ), clusters I-Es and IVs lie on the locus of YMCs. It is interesting to note that cluster IVs lies in a region where extra-Galactic YMCs and present-day Galactic GCs overlap.

It is interesting to analyse the fraction of mass contained in clusters (cluster formation efficiency;  $\Gamma$ ) at different ages in the two observed fields. For this purpose, the masses of the association I-B and cluster IIIs, although only partially sampled by our observations, have been also estimated adopting the same procedures described above. In the *central field*,  $33 \pm 10\%$  of stars younger than 10 Myr are in one of the two major associations (I-A and I-B). This fraction decreases to  $9 \pm 3\%$  if we consider all stars younger than 200 Myr (including all the clusters in this field). A larger fraction has been estimated in the *offset field* ( $19 \pm 6\%$  with  $t < 200$  Myr). For comparison, the fractions of stars in clusters at  $t < 10$  Myr in the samples analysed by Goddard, Bastian & Kennicutt (2010) and Adamo, Östlin, & Zackrisson et al. (2011) range from 4 to 25%, with an increasing trend with the SFR density. Considering the mean SFR of the last 10 Myr in the *central field* ( $\Sigma_{SFR}(< 10 \text{ Myr}) = 0.27 M_{\odot} \text{ yr}^{-1} \text{ kpc}^{-2}$ ), the fraction of stars in clusters estimated here appears to lie slightly above the relation by Goddard et al. (2012), although within the uncertainties. Silva-Villa & Larsen (2011) and Cook et al. (2012) considered an age limit of 100 Myr and a sample of galaxies with SFR densities which are significantly smaller than the averages in our fields ( $\Sigma_{SFR}(< 200 \text{ Myr}) = 0.15$

and  $0.07 M_{\odot} \text{ yr}^{-1} \text{ kpc}^{-2}$  for the *central* and the *offset* field, respectively). Again, they estimated values of  $\Gamma$  on average smaller than those found here. It is worth noting that we calculated  $\Gamma$  including stars in associations which are supposed to dissolve in few Myr. On the other hand, according to the definition given in Sect. 5.3, the criterion to distinguish clusters from associations is based on the comparison between age and dynamical time, this last quantity depending on the system radius. In many previous literature works such a cluster/association discrimination was not possible because of the missing information about radii. So our estimate should be comparable with those available in the literature.

#### 5.4 Mass Function of association I-A

In the resolved association I-A the mass range where a good completeness level is achieved is relatively large ( $27 < M/M_{\odot} < 72$ ). It is therefore possible to estimate the MF of this stellar systems. For this purpose we converted the F330W magnitude (where the MS is clearly separated from the other evolutive sequences) into mass by means of the isochrone which best fits the cluster's CMD. Only MS stars with colours within  $-2 < (F330W - F555W) < -1$  and with  $F330W < 22.4$  have been considered, to avoid contamination from evolved stars and large completeness corrections. For reference, in this color range, the completeness  $\Psi$  is always  $> 50\%$  with  $\Psi \sim 80\%$  at  $F330W=21$  and  $\Psi \sim 90\%$  at  $F330W=20$ . Apparent magnitudes have been transformed into absolute ones adopting the distance modulus and mean reddening reported in Sect. 4.1. To each star a completeness factor has been assigned according to its distance from the center and to its magnitude using the neighbor objects (within 10 px) in the artificial star catalog within 0.25 mag in the F330W and F555W bands. We adopted the method described by Maíz-Apellániz & Úbeda (2005) to bin our data including 20 stars in each bin. The completeness-corrected

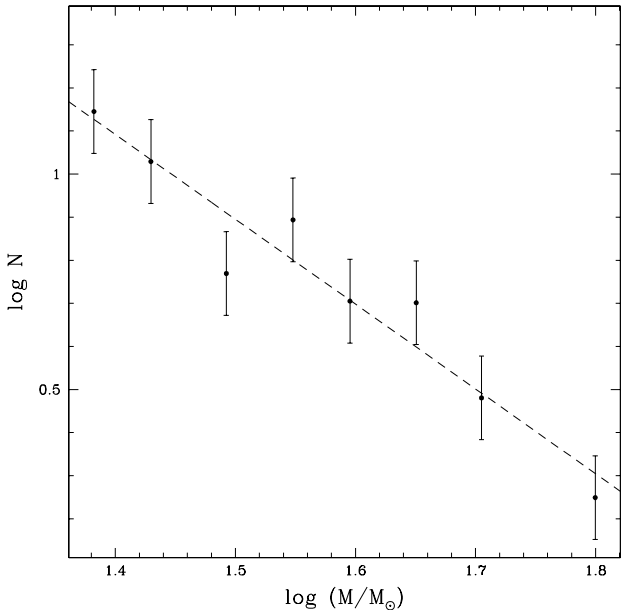


**Figure 14.** MF of association I-A. The best fit power-law (almost corresponding to a Salpeter 1955 law) is marked with a dashed line.

MF for association I-A is shown in Fig. 14. A least-square fit of the observed MF yields a slope of  $\alpha = -1.97 \pm 0.23$ , which is slightly flatter than the Salpeter (1955) law. Consider that the formal uncertainty reported here does not account for all the sources of errors affecting the MF slope determination. A more realistic uncertainty of  $\pm 0.4$  can be estimated according to the relation provided by Weisz et al. (2013b). Unfortunately, such a large uncertainty prevents any firm conclusion on this issue.

The level of mass segregation within association I-A has been estimated by comparing the radial distribution of stars with  $F330W < 21$  with those in the range  $21 < F330W < 22$  (roughly corresponding to masses  $M > 45M_{\odot}$  and  $27 < M/M_{\odot} < 45$ ). The distance of each star has been weighted according to the star completeness as estimated above. It is noticeable that massive stars appear to be more concentrated than less massive ones. However, a Kolmogorov-Smirnov test gives a probability of 8% that the two samples are drawn from the same distribution. So, the above result appears not to be statistically significant. Note that the mass segregation timescale of a  $56 M_{\odot}$  star in such a young cluster is  $t_{ms} = 0.01 t_{rh} = 0.45 Gyr$  (Spitzer 1969; adopting a mean stellar mass of  $\langle m \rangle = 0.57 M_{\odot}$  appropriate for the cluster age and IMF) i.e.  $\sim 180$  times longer than the cluster age.

## 6 DISCUSSION

In this work we studied the stellar population of the most active region of the nearby starburst galaxy NGC 4214 using deep HST images sampling both the field galactic population and five complexes. The SFHs of the field population of the two analysed regions are characterized by the presence of two main bursts occurred within the last 500 Myr: a recent

episode occurred  $\sim 8$  Myr ago, mainly in the central region of the galaxy, and an older one occurred  $\sim 300$  Myr ago which is spread out across a large area. Our analysis does not allow us to sample the oldest (at ages  $> 3 Gyr$ ) galactic population which has been found to dominate the stellar content of this galaxy in previous studies (McQuinn et al. 2010; W11). The spatial distribution of the young ( $\log t/yr < 7.3$ ) and old ( $\log t/yr > 7.3$ ) populations indicate a clumpy SF process with many aggregates of stars displaced in different portions of the field of view according to their ages. The large majority of the young ( $\log t/yr < 7.3$ ) population is located in the innermost region of the galaxy within  $\sim 200$  pc to the galaxy center. The old population is present in both the analysed fields and does not show any significant spatial inhomogeneity. Spatial differences in the SFH have been already noticed in other dwarf irregulars like e.g. the Magellanic Clouds (Weisz et al. 2013a; Cignoni et al. 2013) and NGC 6822 (Gallart et al. 1996). In the above mentioned cases, the regions with strong SF activity are those located in the bar or near the nucleus of these galaxies, well correlated with the HI column density. These variations are generally interpreted as the signature of a recent migration of gas towards the galaxy center which simultaneously shut down star formation in the outer regions while dramatically increasing the star formation rate in the centre. There is a clear correlation between the spatial distribution of clusters and field populations: by adopting the same separation criterion between young/old population ( $\log t/yr \leq 7.3$ ), it is apparent that the two young associations are located within the area where the most intense recent SF activity is present. On the other hand, old YMCs are generally located at large distances from the galactic center (with the exception of cluster I-Es), in regions where only old populations are present. We recall however that the region analysed here covers only the innermost 700 pc of the galaxy and that the SF activity can present a stochastic pattern (Dohm-Palmer et al. 2002).

In spite of the general agreement between data and model CMDs, some differences remain. None of Marigo et al. (2008) models provide an optimal fit for BP and RSG sequences simultaneously. Moreover, as already found in other investigations (see e.g. Larsen et al. 2011) of YMCs, models predict a clear separation between MS and HeB stars in the F555W vs. (F330W-F555W) CMD, while observations do not show such a discontinuity.

We derived accurate ages for the five observed assemblies, while masses and half-light radii have been estimated for three of them. The derived ages span a wide range between  $6.4 < \log t/yr < 8.1$  in agreement with those predicted by recent analyses based on integrated photometry (Úbeda et al. 2007b; Sollima et al. 2013). The youngest associations (I-A and I-B) appear still surrounded by a shell of gas which is being probably expelled by the shocks produced by the supernovae II explosions and/or the wind of very massive stars occurring in these young stellar systems.

By comparing the masses of clusters with the SFR of the surrounding field populations we estimated a cluster formation efficiency of  $\Gamma = 33 \pm 10\%$  in the *central field* within 10 Myr, which decreases when older ( $t < 200$  Myr) populations are considered. The different cluster formation efficiency for the two age selections is partly explained by the infant mortality of clusters which are not able to survive to the gas expulsion phase occurring in the first tens of Myr. This is

also supported by the evidence that the cluster formation efficiency is larger in the *offset field*, where the less dense environment favors the survival of young assemblies. However, the estimated values of  $\Gamma$ , while rather uncertain, follow the empirical relation defined by Goddard et al. (2010) as a function of the SFR density and are larger than those estimated in less active galaxies by Silva-Villa & Larsen (2011) and Cook et al. (2012). This evidence supports the hypothesis that active galaxies form and retain stars in clusters more efficiently than those with a small SFR.

We found no clear signatures of multiple stellar populations in the two resolved associations (I-A and I-B). This is not surprising since, *i*) the number of resolved stars and the uncertainties on the mass function hamper the detection of such subtle features, and *ii*) according to the main proposed scenarios, the second generation of stars should form only after 10-30 Myr after the evolution of rotating massive stars (Decressin et al. 2007) or intermediate mass AGB stars (Ventura et al. 2001).

At face value the mass function of the largest association (I-A) is flatter than the Salpeter (1955) law. A comparison with the compilation by Weisz et al. (2013b) indicates that the slope derived here for this association lies at the bottom envelope of the distribution of their sample (see their Fig. 1). Unfortunately, the intrinsic scatter of the distribution shown by these authors and the large uncertainty of our estimate prevent any conclusion on a possible deviation from a universal Salpeter-like IMF. A hint of mass segregation has been found in this stellar system, although the statistical significance of this evidence is only at  $\sim 2\sigma$ . The dynamical mass-segregation timescale for the considered mass range is more than 2 orders of magnitude longer than the cluster age. So, if confirmed, this evidence would indicate a primordial mass segregation driven by a preferential formation of massive stars in high-density environments (Klessen 2001). Similar evidences have been already found in Galactic associations like the Arches cluster (Stolte et al. 2002), the Orion Nebula Cluster (Hillenbrand & Hartmann 1998), Westerlund 1 (Brandner et al. 2008) and NGC 3603 (Harayama, Eisenhauer & Martins 2008) as well as in a few extra-Galactic YMCs (de Grijs et al. 2002; McCrady, Graham & Vacca 2005; Larsen et al. 2008).

The structural properties of the three objects for which we were able to determine their masses and half-light radii have been compared with those of other low-mass stellar systems. While I-A presents the typical characteristics of large associations, the other two clusters (I-Es and IVs) have masses and half-light radii compatible with those of present-day Galactic GCs and extra-Galactic YMCs. For comparison, YMCs in this mass range have been also observed in nearby starburst galaxies like NGC 1569 (Hunter et al. 2000; Origlia et al. 2001; Larsen et al. 2011), NGC 1705 (Annibali et al. 2009; Larsen et al. 2011), NGC 4449 (Annibali et al. 2011), NGC 1313, NGC 5236 and NGC 7793 (Larsen et al. 2011). The structural evolution of these clusters deserves particular attention. The two youngest associations (I-A and I-B) are still in the phase during which gas expulsion due to the explosions of the first supernovae II is ongoing. This can be deduced by the presence of the shell-shaped gas emission surrounding these stellar systems. A comparison of the dynamical timescale of the association I-A (estimated through the mass and radii derived in Sect. 5.3 and 5.2 and eq. 11

of Portegies-Zwart et al. 2010) with its age indicates a ratio  $t_{age}/t_{dyn} = 0.13$  indicating that it could still not have reached virial equilibrium. Unfortunately, estimates of its velocity dispersion are not available, so it is still not possible to assess the dynamical status of this stellar system. As a consequence of the ongoing gas expulsion and the future mass-loss due to stellar evolution, these young clusters will expand being subject to strong tidally induced mass-loss. The fate of these objects depends on the amount of residual gas still present within the cluster and the strength of the galactic tidal field. For these reasons, it is not clear if they could survive as star clusters for a long time. A different case is that of the older, compact YMCs (I-Es, IIIs and IVs): these objects survived to their initial phase of gas expulsion and will experience only a minor ( $< 10\%$ ) stellar evolution-induced mass-loss. The half-mass relaxation times of clusters I-Es and IVs (calculated using the Spitzer 1969 formula and masses and effective radii listed in Table 1) are  $t_{rh} = 0.46 \text{ Gyr}$  (I-Es) and  $t_{rh} = 1.63 \text{ Gyr}$  (IVs) i.e. comparable to those of present-day GCs (McLaughlin & van der Marel 2005). The evaporation timescale for these clusters ( $t_{ev} \sim 140 t_{rh}$ ; Spitzer 1940) turns out to be larger than the Hubble time. N-body simulations by Madrid, Hurley & Sippel (2012) indicate that the future structural evolution of these stellar systems will be determined by the strength of the tidal field which drives both the fraction of mass-loss and the evolution of the half-mass radius. In this regard, it is important to note that both clusters have large central concentrations, which make them more resistant to tidal effects. Cluster I-Es is located close to the center of NGC 4214 and has a relatively small mass, so it is unlikely that it could maintain a GC-like mass. On the other hand, cluster IVs is more distant from the galactic center and has a mass and size similar to those of present-day Galactic GCs (see Fig. 13). Under these conditions, its mass and radius are expected to be only marginally affected by the weak tidal field of NGC 4214 and could therefore evolve toward a GC-like structure.

## ACKNOWLEDGMENTS

AB, RG and SL acknowledge the PRIN INAF 2009 "Formation and Early Evolution of Massive star Clusters" (PI R. Gratton); AS, SL acknowledge the PRIN INAF 2011 "Multiple populations in globular clusters: their role in the Galaxy assembly" (PI E. Carretta); and MT, AB, and SL acknowledge the PRIN MIUR 2010-2011 "The Chemical and Dynamical Evolution of the Milky Way and Local Group Galaxies" (PI F. Matteucci), prot. 2010LY5N2T. We thank the anonymous referee for his/her helpful comments and suggestions.

## REFERENCES

- Adamo A., Östlin G., Zackrisson E., 2011, MNRAS, 417, 1904
- Aloisi A., Tosi M., Greggio L., 1999, AJ, 118, 302
- Andrews J. E., et al., 2013, ApJ, 767, 51
- Annibali F., Tosi M., Monelli M., Sirianni M., Montegriffo P., Aloisi A., Greggio L., 2009, AJ, 138, 169
- Annibali F., Tosi M., Aloisi A., van der Marel R. P., 2011, AJ, 142, 129

- Arp H., Sandage A., 1985, *AJ*, 90, 1163
- Beck S. C., Turner J. L., Kovo O., 2000, *AJ*, 120, 244
- Beerman L. C., et al., 2012, *ApJ*, 760, 104
- Billett O. H., Hunter D. A., Elmegreen B. G., 2002, *AJ*, 123, 1454
- Brandner W., Clark J. S., Stolte A., Waters R., Negueruela I., Goodwin S. P., 2008, *A&A*, 478, 137
- Chiosi C., 1998, *Stellar astrophysics for the local group: VIII Canary Islands Winter School of Astrophysics*, 1
- Cignoni M., Cole A. A., Tosi M., Gallagher J. S., Sabbi E., Anderson J., Grebel E. K., Nota A., 2012, *ApJ*, 754, 130
- Cignoni M., Cole A. A., Tosi M., Gallagher J. S., Sabbi E., Anderson J., Grebel E. K., Nota A., 2013, *ApJ*, 775, 83
- Cole A. A., et al., 2007, *ApJ*, 659, L17
- Cook D. O., et al., 2012, *ApJ*, 751, 100
- Dalcanton J. J., et al., 2009, *ApJS*, 183, 67
- Davies B., Figer D. F., Kudritzki R.-P., MacKenty J., Najarro F., Herrero A., 2007, *ApJ*, 671, 781
- D'Ercole A., Vesperini E., D'Antona F., McMillan S. L. W., Recchi S., 2008, *MNRAS*, 391, 825
- Decressin T., Meynet G., Charbonnel C., Prantzos N., Ekström S., 2007, *A&A*, 464, 1029
- de Grijs R., Gilmore G. F., Johnson R. A., Mackey A. D., 2002, *MNRAS*, 331, 245
- de Vaucouleurs G., de Vaucouleurs A., Corwin H. G. Jr., Buta R. J., Paturel G., Fouqu e P., 1991, *Third Reference Catalogue of Bright Galaxies. Volume I-III*, Springer eds., New York, NY (USA)
- Dohm-Palmer R. C., Skillman E. D., Mateo M., Saha A., Dolphin A., Tolstoy E., Gallagher J. S., Cole A. A., 2002, *AJ*, 123, 813
- Ekstr m S., et al., 2012, *A&A*, 537, A146
- Fanelli M. N., et al., 1997, *ApJ*, 481, 735
- Figer D. F., Kim S. S., Morris M., Serabyn E., Rich R. M., McLean I. S., 1999, *ApJ*, 525, 750
- Figer, D. F., MacKenty, J. W., Robberto, M., Smith K., Najarro F., Kudritzki R. P., Herrero A., 2006, *ApJ*, 643, 1166
- Fouesneau M., Lan on A., 2010, *A&A*, 521, A22
- Frenk C. S., White S. D. M., Davis M., Efstathiou G., 1988, *ApJ*, 327, 507
- Gallart C., Aparicio A., Bertelli G., Chiosi C., 1996, *AJ*, 112, 2596
- Garc a-Benito R., P rez-Montero E., 2012, *MNRAS*, 423, 406
- Girardi L., et al., 2008, *PASP*, 120, 583
- Goddard Q. E., Bastian N., Kennicutt R. C., 2010, *MNRAS*, 405, 857
- Greggio L., Tosi M., Clampin M., de Marchi G., Leitherer C., Nota A., Sirianni M., 1998, *ApJ*, 504, 725
- Gunawardhana M. L. P., et al., 2011, *MNRAS*, 415, 1647
- Harayama Y., Eisenhauer F., Martins F., 2008, *ApJ*, 675, 1319
- Hillenbrand L. A., Hartmann L. W., 1998, *ApJ*, 492, 540
- Hoversten E. A., Glazebrook K., 2008, *Apj*, 675, 163
- Hunter D. A., O'Connell R. W., Gallagher J. S., Smecker-Hane T. A., 2000, *AJ*, 120, 2383
- Karachentsev I. D., Karachentseva V. E., Huchtmeier W. K., Makarov D. I., 2004, *AJ*, 127, 2031
- King I. R., 1962, *AJ*, 67, 471
- King I. R., 1966, *AJ*, 71, 64
- Klessen R. S., 2001, *ApJ*, 556, 837
- Kobulnicky H. A., Skillman E. D., 1996, *ApJ*, 471, 211
- Krist J., Hook R., Stoehr F., 2010, *Astrophysics Source Code Library*, 10057
- Kroupa P., 2001, *MNRAS*, 322, 231
- Kruijssen J. M. D., 2009, *A&A*, 507, 1409
- Kruijssen J. M. D., 2012, *MNRAS*, 426, 3008
- Larsen S. S., Richtler T., 2000, *A&A*, 354, 836
- Larsen S. S., 1999, *A&AS*, 139, 393
- Larsen S. S., Brodie J. P., Huchra J. P., Forbes D. A., Grillmair C. J., 2001, *AJ*, 121, 2974
- Larsen S. S., Origlia L., Brodie J., Gallagher J. S., 2008, *MNRAS*, 383, 263
- Larsen S. S., et al., 2011, *A&A*, 532, A147
- Lee J. C., et al., 2009, *Apj*, 706, 599
- MacKenty J. W., Ma z-Apell niz J., Pickens C. E., Norman C. A., Walborn N. R., 2000, *AJ*, 120, 3007
- Madrid J. P., Hurley J. R., Sippel A. C., 2012, *ApJ*, 756, 167
- Ma z-Apell niz J., Mas-Hesse J. M., Munoz-Tunon C., Vilchez J. M., Castaneda H. O., 1998, *A&A*, 329, 409
- Ma z Apell niz J.,  beda L., 2005, *ApJ*, 629, 873
- Marigo P., Girardi L., Bressan A., Groenewegen M. A. T., Silva L., Granato G. L., 2008, *A&A*, 482, 883
- McCraday N., Graham J. R., Vacca W. D., 2005, *ApJ*, 621, 278
- McLaughlin D. E., van der Marel R. P., 2005, *ApJS*, 161, 304
- McQuinn K. B. W., Skillman E. D., Dalcanton J. J., Dolphin A. E., Holtzman J., Weisz D. R., Williams B. F., 2011, *ApJ*, 740, 48
- Melbourne J., et al., 2012, *ApJ*, 748, 47
- Meurer G. R., et al., 2009, *Apj*, 695, 765
- Origlia L., Leitherer C., Aloisi A., Greggio L., Tosi M., 2001, *AJ*, 122, 815
- Parmentier G., Goodwin S. P., Kroupa P., Baumgardt H., 2008, *ApJ*, 678, 347
- Perina S., et al., 2010, *A&A*, 511, A23
- Piskunov A. E., Schilbach E., Kharchenko N. V., R ser S., Scholz R.-D., 2007, *A&A*, 468, 151
- Popescu B., Hanson M. M., 2010, *ApJ*, 713, L21
- Portegies Zwart S. F., McMillan S. L. W., Gieles M., 2010, *ARA&A*, 48, 431
- Rockosi C. M., et al., 2002, *AJ*, 124, 349
- Salasnich B., Bressan A., Chiosi C., 1999, *A&A*, 342, 131
- Salpeter E. E., 1955, *ApJ*, 121, 161
- Sandage A., Bedke J., 1994, *The Carnegie Atlas of Galaxies. Volumes I, II*, Carnegie Institution of Washington Publ., No. 638
- Schaller G., Schaerer D., Meynet G., Maeder A., 1992, *A&AS*, 96, 269
- Schlegel D. J., Finkbeiner D. P., Davis M., 1998, *ApJ*, 500, 525
- Silva-Villa E., Larsen S. S., 2011, *A&A*, 529, A25
- Silva-Villa E., Larsen S. S., 2012, *MNRAS*, 423, 213
- Silverman B. W., 1986, *Monographs on Statistics and Applied Probability*, London: Chapman and Hall, 1986
- Sirianni M., et al., 2005, *PASP*, 117, 1049
- Sollima A., Gratton R. G., Carretta E., Bragaglia A., Lucatello S., 2013, *MNRAS*, 433, 1276
- Spitzer L. Jr., 1940, *MNRAS*, 100, 396
- Spitzer L., Jr., 1969, *ApJL*, 158, L139
- Stetson P. B., 1987, *PASP*, 99, 191
- Stolte A., Grebel E. K., Brandner W., Figer D. F., 2002, *A&A*, 394, 459
- Tolstoy E., Hill V., Tosi M., 2009, *ARA&A*, 47, 371
- Tutukov A. V., 1978, *A&A*, 70, 57
-  beda L., Ma z-Apell niz J., MacKenty J. W., 2007b, *AJ*, 133, 917
-  beda L., Ma z-Apell niz J., MacKenty J. W., 2007a, *AJ*, 133, 932
- Ventura P., D'Antona F., Mazzitelli I., Gratton R., 2001, *ApJL*, 550, L65
- Vieira, J. D., et al., 2013, *Nature*, 495, 344
- Weisz D. R., et al., 2011, *ApJ*, 743, 8
- Weisz D. R., Dolphin A. E., Skillman E. D., Holtzman J., Dalcanton J. J., Cole A. A., Neary K., 2013, *MNRAS*, 431, 364
- Weisz D. R., et al., 2013, *ApJ*, 762, 123
- White S. D. M., Rees M. J., 1978, *MNRAS*, 183, 341
- Williams B. F., Dalcanton J. J., Gilbert K. M., Seth A. C., Weisz D. R., Skillman E. D., Dolphin A. E., 2011, *ApJ*, 735, 22